Die Soldering: Mechanism of the Interface Reaction between Molten Aluminum Alloy and Tool Steel

SUMANTH SHANKAR and DIRAN APELIAN

Die soldering is the result when molten aluminum sticks to the surface of the die material and remains there after the ejection of the part; it results in considerable economic and production losses in the casting industry, and is a major quality detractor. In order to alleviate or mitigate die soldering, one must have a thorough understanding of the mechanism by which the aluminum sticks to the die material. A key question is whether the die soldering reaction is diffusion controlled or interface controlled. A set of diffusion couple experiments between molten aluminum alloy and the ferrous die was carried out. The results of the diffusion couple experiments showed that soldering is a diffusional process. When aluminum comes in contact with the ferrous die material, the iron and the aluminum atoms diffuse into each other resulting in the formation of a series of intermetallic phases over the die material. Initially iron and aluminum react with each other to form binary iron-aluminum intermetallic phases. Subsequently, these phases react with the molten aluminum to further form ternary iron-aluminum-silicon intermetallic phases. Iron and aluminum have a great affinity for each other and the root cause of die soldering is the high reaction kinetics, which exists between iron and aluminum. Once the initial binary and ternary intermetallic phase layers are formed over the die material, the aluminum sticks to the die due to the abnormally low thermal conductivity of the intermetallic phases, and due to favorable interface energies between the intermetallic layers and aluminum. The experimental details, the results of the interface reactions, and the analysis leading to the establishment of the mechanism giving rise to die soldering are reviewed discussed.

I. INTRODUCTION

DIE soldering, or die sticking, is a casting defect in which molten metal "welds" to the surface of the metallic die mold during the casting process. The defect is prevalent in aluminum die casting and permanent mold-casting industries. The cast-aluminum alloy sticks to the tool steel-die material and remains there even after ejection of the casting. Subsequent casting suffer from dimensional and surface finish issues; die soldering is a quality detractor. As a remedial measure, the casting operation is stopped to repair or replace the die. Previous work[1–10] has not alleviated the problem, and the issue of die soldering remains to be a serious detractor in the casting industry.

Die soldering is the result of an interface reaction between the molten aluminum and the die material. Aluminum 380 alloy and H-13 die steel are the most prevalent melt and die material used in aluminum die casting. Figure 1 is an illustration of the harsh environment that is present during the die casting process. The molten metal is shot in through the gate of the die at high pressures, temperatures, and velocities. The casting cycles are generally less than 1 minute. Hence, the die surface is subjected to repeated shots of aluminum melt resulting is excessive wear. This results in damages to the die surface coating and the lubricant. Subsequently, the steel surface of the die comes in contact with the aluminum melt. The aluminum attacks the weak regions in the steel microstructure, and erosion pits form. The iron from the steel diffuses into the aluminum melt resulting in the formation of intermediate layers of binary Fe-Al and ternary Fe-Al-Si phases. Once these phases consolidate and prevent further aluminum-steel contact, the aluminum sticks to them and results in soldering. Figure 2 shows a schematic of the cross section of a soldered die steel-aluminum interface.

The aim of this publication is to establish a mechanism for die soldering. The microstructural features of the soldering interface are reviewed and discussed. The various intermediate compounds found in the soldering microstructure are identified through scanning electron microscopy (SEM), energy dispersive X-ray spectroscopy (EDX), and X-ray diffraction techniques. Moreover, the analysis presented here gives an understanding of the nature and kinetics of the growth of the intermediate compounds, which extend beyond the soldered layer. The results of the experiments clearly indicate that soldering is a diffusion-driven reaction—the iron diffusing out of the tool steel into the molten aluminum and forming the intermediate layers. The role of the various different alloying elements in molten aluminum during soldering has also been investigated and analyzed.

II. BACKGROUND

Extensive metallographic analysis of soldered interfaces between aluminum and H-13 tool steel die was performed.[11] Samples were obtained from commercial die casters* with full documentation on the samples. These examinations revealed the existence of a series of intermediate phases

SUMANTH SHANKAR, Postdoctoral Fellow, and DIRAN APELIAN, Professor and Head, are with the Advanced Casting Research Center, Metal Processing Institute, WPI, Worcester, MA 01609. Contact e-mail: dapelian@wpi.edu

Manuscript submitted August 17, 2001.

*Cambridge Tools and Manufacturing, Burlington, MA; GM-Powertrain, Bedford, IN; Lester Precision Die Casting, Solon, OH; and Madison-Kipp, Madison WI.

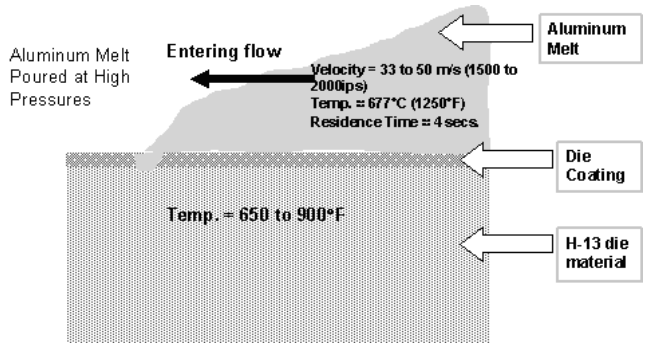

Fig. 1—Schematic diagram of the harsh process environment that exists during die casting leading to die soldering.

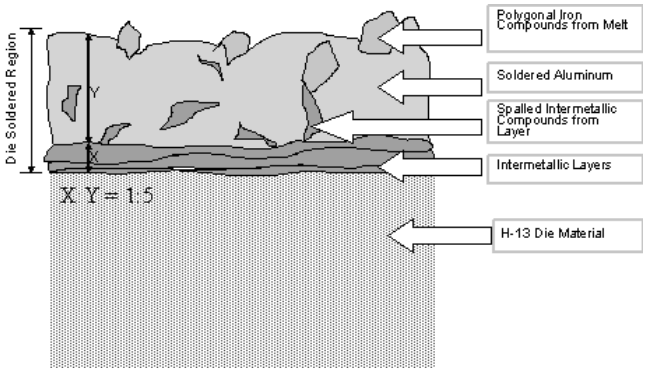

Fig. 2—Schematic of a typical die soldering cross section, showing the intermediate layers, soldered aluminum, and spalled intermetallic floats

between the surface of the tool steel and the soldered aluminum. The results revealed quite an interesting feature in die soldering; irrespective of the process conditions (time, temperature, and die surface area), there was a consistent specific ratio of 1:5 between the thickness of the intermediate layer and that of the total soldered layer.[12] Even though this ratio remained constant, the nature and thickness of the intermediate layers did change when the die material or the aluminum alloy composition changed.[13] Thus, the role of the intermediate layers formed during die soldering is critical in establishing the overall mechanism. A critical literature search was carried out focusing on the compositional effects of the aluminum melt and die and the thermodynamics and kinetics of die soldering.

Hot-dip aluminizing of steel is a process where the goal is to have the aluminum stick to the steel strip substrate. Our initial studies[11] indicated that the nature and thickness of the intermediate phases formed in a soldered cross section was similar to that formed during aluminizing of steel. Thus, it will be relevant to review the literature on aluminizing of steel as it will shed insight into the die soldering process. Several researchers[14–23] have observed and established the nature of these intermediate layers along with their growth kinetics. There are two methods to aluminize a steel sheet. Type 1 processes use aluminum-silicon melt to coat, while pure aluminum melt is used in the Type 2 processes. Most of the work done in aluminizing considered a plain carbon steel or iron sheet coated with aluminum. However, in casting, the die surface is typically H-13 tool steel, and the alloy is typically an aluminum-silicon alloy with various other

Table I. Phase Identities in Fe-Al-Si System[8]

		Composition, Wt Pct		
Nomenclature	Stoichiometry	Fe	Al	Si
τ_1	$Fe_3Si_2Al_3$	55	26.6	18.4
τ_2	$Fe_6Si_5Al_{12}$	41.9	40.5	17.6
τ_3	$Fe_6Si_5Al_9$	42.1	36.6	21.2
τ_4	$FeSi_2Al_3$	28.9	41.9	29.1
τ_5	$Fe_6Si_6Al_5$	38.1	46.0	16.0
τ_6	$FeSiAl_4$	29.1	56.3	14.6

additive elements. Moreover, the intermediate compounds formed in a soldered cross section result from a multicomponent diffusion-couple reaction containing H-13 tool steel at one end and an aluminum-silicon alloy melt at the other, rather than a single component system as is the case in aluminizing of steel. The nature of the diffusion process seems to be similar in both of these processes, but the composition and the thickness of the intermediate phase layers are different.

Wladyslaw and Alexander[10] observed that the mechanism of soldering is not an electrochemical one but that it is purely based on the diffusion and chemical reactions of the elements in the die (solid) and the liquid metal. Experienced aluminum die casters have observed that different grades of aluminum alloys differ from each other in their tendency towards soldering. According to Wladyslaw and Alexander[10] aluminum exhibits a strong adhesive tendency to stick to iron. In their experiments using auger electron spectroscopy and electron spectroscopy for chemical analysis (ESCA) photoelectron spectroscopy, they showed the existence of an intermediate layer consisting of zones of intermetallic compounds, such as Fe_2Al_5 (prevalent), Fe_3Al, and $FeAl_3$ phases. On the other hand, the presence of other alloying elements, such as Si, Cu, Mg, *etc.*, resulted in the formation of a number of complex intermetallic compounds in the intermediate alloy layer. Wladyslaw and Alexander also established that the soldering tendency of the primary aluminum metal is the greatest, followed by that of the Al-Mg alloy, the hypoeutectic Al-Si alloy, the Al-Si-Cu, and the eutectic Al-Si, which has the least soldering tendency. Increasing amounts of silicon in the aluminum decreased the growth rate of the intermetallic layers. Takeda and Mutazaki[8] gave a comprehensive list of all the intermetallic compounds that can be formed in an aluminum-iron-silicon system. These are tabulated in Table I and present a qualitative understanding of the possible intermediate compounds that can be formed in an iron-aluminum-silicon ternary system.

Carrying out SEM analysis of aluminized samples with Al-10 wt pct Si alloy (Type I process), Denner and Kim[15] have shown that for short immersion times, in the order of 5 seconds, the θ-$FeAl_3$ initially forms as a very thin layer at the steel interface. This is immediately followed by the formation of the η-Fe_2Al_5 layer, and as this layer grows, it contains isolated and nonisolated particles of θ-$FeAl_3$. Both of these phases contain an elemental silicon phase. In the presence of silicon in the aluminum, the η-Fe_2Al_5 layer is followed by the formation of the τ_5-Fe_2SiAl_7 layer. The τ_5 layer is then followed by the formation of coexisting layers of τ_6 and τ_2 intermetallic phases. Lastly, aluminum gets coated above all these intermediate layers. The aluminum

coat contains raftlike particles that are predominantly composed of the τ_6 and τ_2 intermetallic compounds. Not surprisingly, the composition of the intermediate layer in aluminized steel is similar to that found in die-soldered microstructures.

In contrast, when there is no silicon present in the aluminum melt, the interaction of the melt and the steel surface is quite different. In the Type 2 aluminizing process, the steel-alloy layer interface is highly corrugated, and the Fe-Al intermetallic compounds are the only ones that are formed. Here, the aluminum coat is much thinner compared to that of the intermetallic layers, while in Type 1 process, the intermetallic layer is thinner.[14,16]

The reason why silicon retards the growth of the alloy layer is controversial. Nicholls[17] and Heumann and Dittrich[18] are of the view that aluminum is the chief diffusing species in the Type 2 aluminizing process. They rationalize that silicon atoms occupy the structural vacancies of the η-Fe_2Al_5 phase, which occurs in the Type 1 process; whereas in Type 2 process, aluminum diffusion is promoted because of the absence of silicon. On the other hand, Lainer *et al.*[23] conclude that the effect of silicon arises from the formation of Fe-Si-Al ternary phases, which nucleate and grow at a slower rate than η-Fe_2Al_5. These authors strongly dispute Nicholls'[17] view that aluminum is the primary diffusing species in the Type 2 aluminizing process. Based on a few solid-state diffusion experiments, they claim that iron is the faster diffusing species. Subsequently, Kurakin and Fiz[19] stated that the primary diffusing species in the Type 2 process was iron and that in the Type 1 process, it was aluminum. This was explained in terms of the disruption of steel/η-Fe_2Al_5 interfacial contact in Type 2 aluminizing. This is not apparent in Type 1 aluminizing, where silicon retards the growth of this phase. Komatsu *et al.*[20] and Denner *et al.*[15] subscribe to the viewpoint that the silicon accelerates the velocity of the iron enrichment in aluminum melts. Eggeler *et al.*[16] conducted coating experiments that convincingly proved that the iron enrichment theory is not valid. They also confirmed that silicon influences the diffusion conditions in the η-Fe_2Al_5 phase.

Studying the parameters that have a deleterious effect on the aluminizing process is critical to understanding die soldering. For example, there are various alloying elements that can be added to the aluminum melt that will either increase or decrease the thickness of the intermediate layer. Unfortunately, the aluminizing literature does not offer a clear and comprehensive theory that can be applied to die soldering. By extending the theory proposed by Akdaniz *et al.*,[24] the role of these elements in affecting the activity coefficients of the diffusing species in the intermetallic layers can be determined from the general equation developed by Wagner.[25]

$$\mu_i^{\text{excess}} = \text{R}T \ln \gamma_\text{i} \quad [1]$$

$$\ln \gamma_\text{i} = \ln \gamma_\text{i}^0 + \Sigma \varepsilon_\text{i}^{(\text{j})} C_\text{j} \quad [2]$$

where γ_i^0 is a constant and is independent of concentration of constituent elements in the intermetallic layers. The subscript i can be substituted by any element in the layer. The γ_i is the activity coefficient of element i, and $\varepsilon_\text{i}^\text{j}$ is the interatomic interaction parameters of the element i due to element j. The c_j is the atomic concentration of the element j in the intermetallic layers.

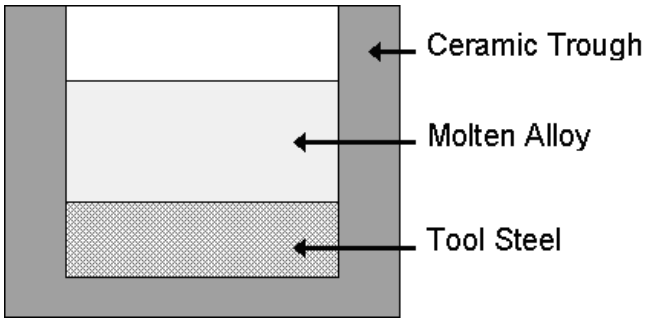

Fig. 3—Schematic diagram showing the setup of the diffusion couple between the die material and the molten aluminum alloy

The behavior of these elements is exemplified by the theory proposed by Akdaniz *et al.*[24] For example, at a temperature of 800 °C, the value of $(\varepsilon_{\text{Al}}^{\text{Si}} C_{\text{Si}}) + (\varepsilon_{\text{Al}}^{\text{Al}} C_{\text{Al}})$ in Eq. [2] is −2397.59. This value was calculated from the activity coefficients of Al in a layer of intermetallic compounds consisting of $Fe_{95}(Al_{100-x}Si_x)_5$ alloys, with 1 at. pct of Si_x. For this condition, the value of (γ_{Al}) in Eq. [2] is a small fraction, and thus, the chemical potential of aluminum given by Eq. [1] is decreased due to the presence of silicon. It can be concluded, therefore, that diffusion of aluminum in an intermetallic layer containing silicon is negligible compared to one without silicon. A similar analysis can be performed to demonstrate the effects of various other elements on the chemical potential of aluminum in the intermetallic layers.

Iron content in the casting alloy plays a very crucial role in causing soldering. According to Norström and Klarenfiord,[8] the maximum solubility of iron in aluminum is 3 wt pct at 700 °C. The soldering phenomenon decreases as the iron content approaches the maximum solubility value. Also, the iron content influences the growth of the intermediate layer, which has a direct influence on soldering. Holz[26] found that the soldering tendency of an alloy with 0.8 wt pct iron is high and that of an alloy with 1.1 wt pct iron is very low. This is because as the iron content in the cast metal reaches its saturation level, the chemical potential gradient, which is the driving force for the diffusion of the iron atoms from the die to melt, is greatly reduced.

Though the literature search was helpful in a qualitative understanding of the role of alloying elements in the molten metal, the work to date does not offer a quantitative understanding. A mechanism of die soldering is needed to be able to control the process.

III. EXPERIMENTS

The intermediate layers that are formed at the tool steel and molten aluminum interface are the result of a diffusional process wherein the iron atoms diffuse out of the tool steel into the aluminum melt. However, whether it is an interface-controlled or a diffusion-controlled process can only be determined by performing multicomponent diffusion-couple experiments. Figure 3 shows a schematic diagram of the experimental setup used for the diffusion-couple experiments.

In this set of experiments, a disk of H-13 die material of dimensions 0.75-in. diameter and 0.25-in. high was taken and preheated to 325 °C. The surface of the H-13 steel disk

had been polished to a 325-grit finish. Half of the polished surface was coated with a layer of white boron-nitride paste to prevent the aluminum from interacting with the steel substrate. This coated area of the surface was used as a reference point to measure the depth of attack on the steel surface by molten aluminum. The die material sample was then placed in a ceramic trough of diameter 0.75 in. such that there was a negligible gap between the walls of the trough and the cylindrical sample. Aluminum melt was then poured into the trough over the steel surface, and the system was left undisturbed in a furnace maintained at 625 °C. The melt used in the experiment was industrial grade 380.1 alloy. The diffusion couple was kept for three different times of 48, 120, and 168 hours, and subsequently, the samples were quenched in cold water to arrest any further reaction. Furthermore, three samples were sectioned for metallographic analysis for each of the different diffusion times.

Three samples from each of these die-soldered interfaces were metallographically examined. Specifically:

(1) Scanning electron microscopy was performed on the samples for both a quantitative and qualitative understanding of the various phases that formed during the diffusion process. The distribution of all the phases and elements present in the diffusion zone was determined. This was accomplished *via* extensive X-ray mapping of all the elements in the diffusion zone.
(2) A second sample from each of the experimental runs was used to evaluate the structure and stoichiometry of the various phases present in the intermediate compound layers. The intermetallic compounds were stripped out of the steel surface and were crushed into a fine powder, which was then mounted on a glass plate. X-ray diffraction patterns were then obtained to establish the identity of the intermetallic phases present in the diffusion zone.
(3) A third sample from each of the experimental runs was used to determine the sequence in which the identified intermetallic-compound layers appeared in the diffusion zone. Sample cross sections were ground and polished at an angle of less than 5 deg. This enabled the intermetallic layers to have a larger area projected onto the X-ray beam in the goniometer. The samples were then evaluated by the X-ray diffractometer, and phases were identified in the order in which they appeared in the diffusion zone. The scan rate of the X-ray diffractometer was 0.5 degrees/min, and the count time was 4 seconds at each angle. The aperture of the beam was 3 deg for the powder sample and 0.1 deg for the slant-polished intermediate layers. A chromium tube was used to enhance the peaks in the aluminum side of the spectrum. The range of angle scanned was 25 to 165 deg.

In addition to the metallographic analyses of controlled die-soldered laboratory samples, microstructure and metallographic analyses were carried out on die-soldered samples obtained from the industrial sector to verify and validate the results.

IV. RESULTS

Figure 4 shows the microstructures obtained from the interaction between H-13 and aluminum melt from various

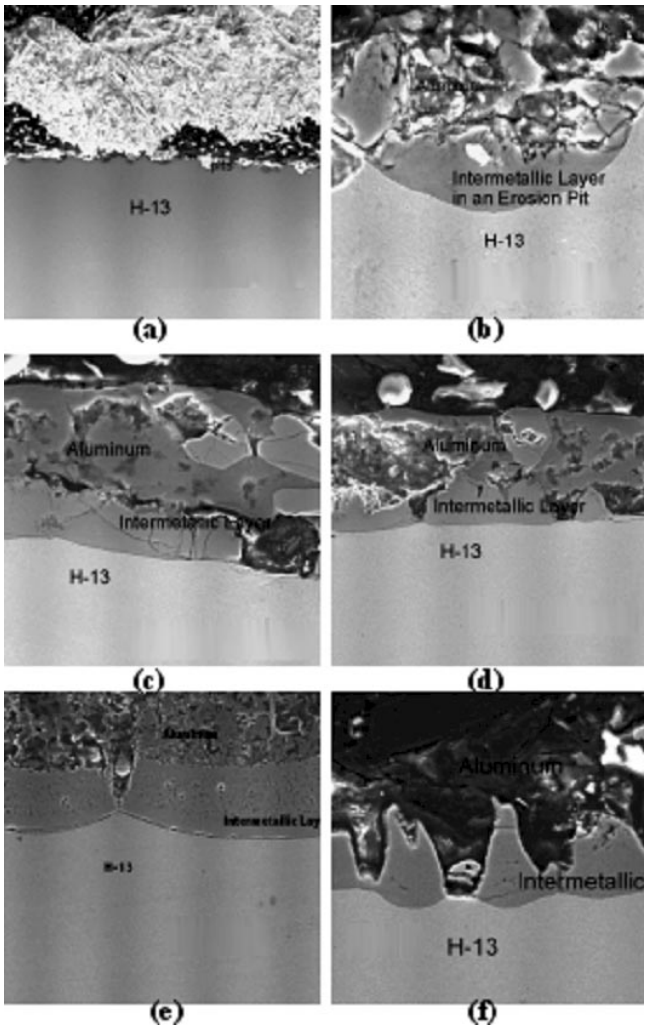

Fig. 4—Selected microstructures from experimental laboratory trial runs (L-16 experimental matrix). (*a*) Pits formed on the surface of the H-13 die steel due to repeated attack by molten aluminum. (*b*) Close up of the formation of the initial intermediate phase layers on the pits. (*c*) and (*d*) Straightening out of pits and subsequent joining of the adjacent intermediate phase layers. (*e*) Gaps between pits through which molten aluminum from subsequent cast shots enters and reacts with the H-13 die steel. (*f*) Pyramid shaped intermediate phase layers that grow out of the pits on the die surface. These pyramids expand along the steel surface and merge with each other to form one continuous intermediate layer.

experiments carried out in the laboratory. The microstructural features in Figure 4 are representative of the key features observed in most of the specimens in the L-16 experimental matrix. Figure 5 shows the microstructures of soldered samples obtained from industrial sites. These micrographs clearly show the pitting behavior on the steel surface.

Figure 4(a) shows the formation of initial pits on the surface of the H-13 steel due to aluminum attack. Figure 4(b) is a closeup on one of the pits seen in Figure 4(a), showing the formation of the initial intermetallic phases between iron and aluminum (mostly binary phases). Also, observed is the eroded steel surface floating in the aluminum layer. The spalled steel phase also reacts with aluminum to give raftlike intermetallic phases. Figure 4(c) shows the pitting in an advanced stage for the same time due to variations in alloy chemistry. The intermediate phases have grown

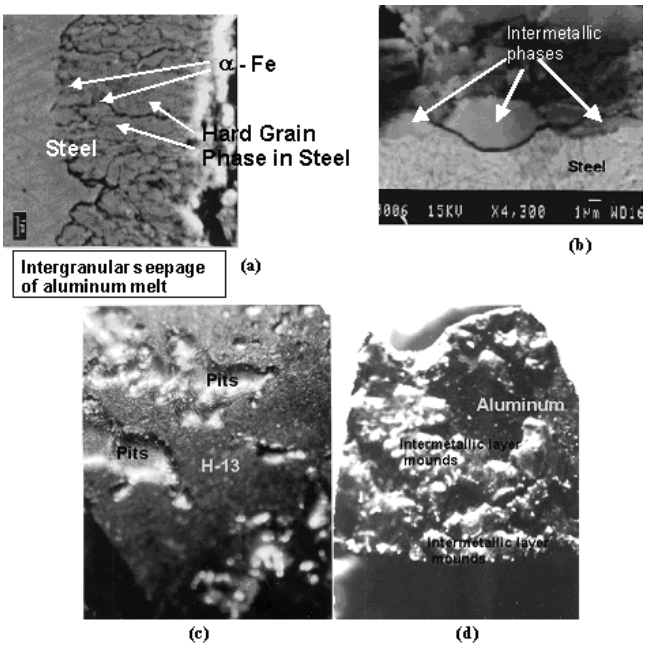

Fig. 5—Microstructures of soldered samples obtained from a commercial die casting operation. (*a*) Initial attack of the softer intergranular regions on the surface of the die steel by molten aluminum. (*b*) Formation of the subsequent pits after the grain boundary erosion. It also shows the formation of the initial phases in the intermediate layer inside these pits. (*c*) and (*d*) Stereomicrograph of the pits on the surface of an H-13 die material and the counterpart soldered aluminum surface containing mounds of intermediate phases that fit into the pits on the steel surface.

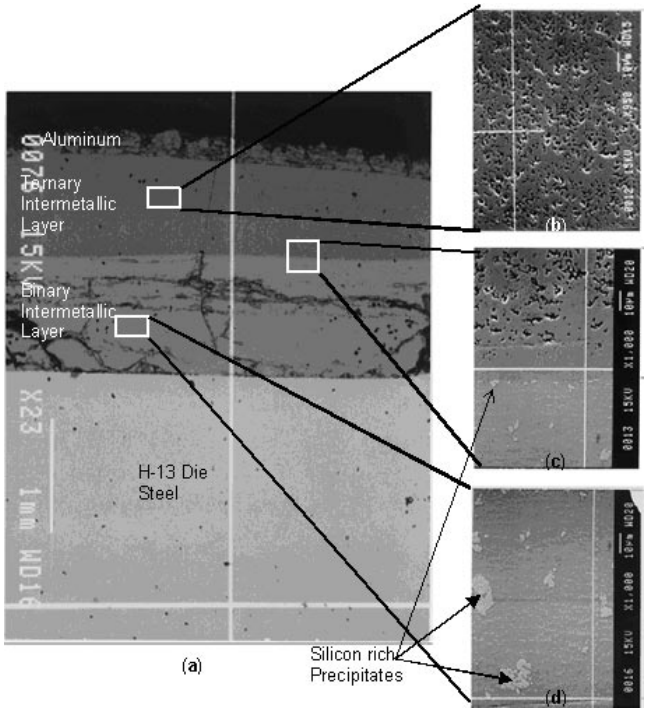

Fig. 6—Micrographs showing the microstructure of the diffusion couple. Time of reaction was 1 week (168 h). There are three layers of intermetallic phases between the aluminum alloy and steel surface: the ternary α-(Al,Fe,Si) phase layer (Fig. (b)); the intermediate θ-Fe_4Al_{13} layer (Fig. (c)); and the binary η-Fe_2Al_5 layer (Fig. (d)). Micrographs (b), (c), and (d) show magnified portions in (a).

considerably, and soldering is more defined. Notice the raft-like steel phases floating in aluminum have undergone complete reaction and have changed into intermetallic phases. In Figure 4(d), the pits have become more developed. Radial growth of the intermetallic phases gives rise to pyramid-shaped intermetallic layers over the pits due to iron diffusion. A well-defined and compact intermediate-phase layer is observed in Figure 4(e); moreover, the pits are straightening. The sole contact between molten aluminum and steel is through the gaps between adjacent pits. Initial formation of pyramid-shaped intermetallic phase from the pits can be noticed in Figure 4(f); this is due to iron diffusion. In all the microstructures, the top porous layer of the intermetallic phase is primarily α-(Fe,Al,Si) phase, whereas the bottom compact layer is primarily η-Fe_2Al_5 and other binary iron-aluminum phases. The phase identities have been validated along with the results of the diffusion-couple experiments and the X-ray diffractometer analysis.

In Figure 5, the die material is H-13, and the aluminum alloy is 380.1. Figure 5(a) shows the phase boundary erosion of the steel surface by the aluminum melt. The grains loosened by the aluminum results in the formation of erosion pits and eventually the formation of binary Fe-Al phases. Figure 5(b) shows the next stage after phase boundary erosion: the formation of erosion pits and the subsequent formation of the binary Fe-Al phases in these pits. In addition, some eroded portions of the die material surface can be seen floating above the pits.

Figure 5(c) is a stereo micrograph (50X) showing the erosion pits on the H-13 steel surface. Figure 5(d) is the

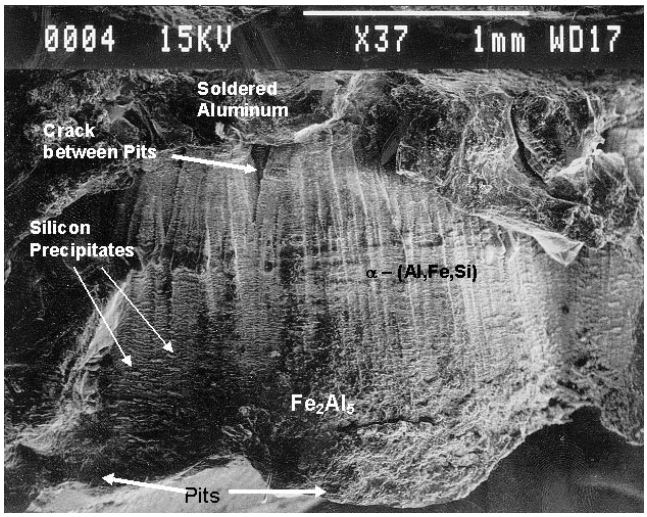

Fig. 7—Cross section of the intermetallic layer that was formed in the diffusion couple experiment (1 week).

counterpart of Figure 5(c), wherein the mounds of intermetallic phases are found on the surface of the soldered aluminum in contact with the steel surface. Figures 5(c) and (d) are also micrographs of soldered samples, obtained from industries, where the intermetallic layers were mechanically stripped out of the steel surface.

Figures 6 and 7 show representative microstructures from the cross section of the diffusion couple. These samples had undergone 168 hours of diffusion reaction. The die material

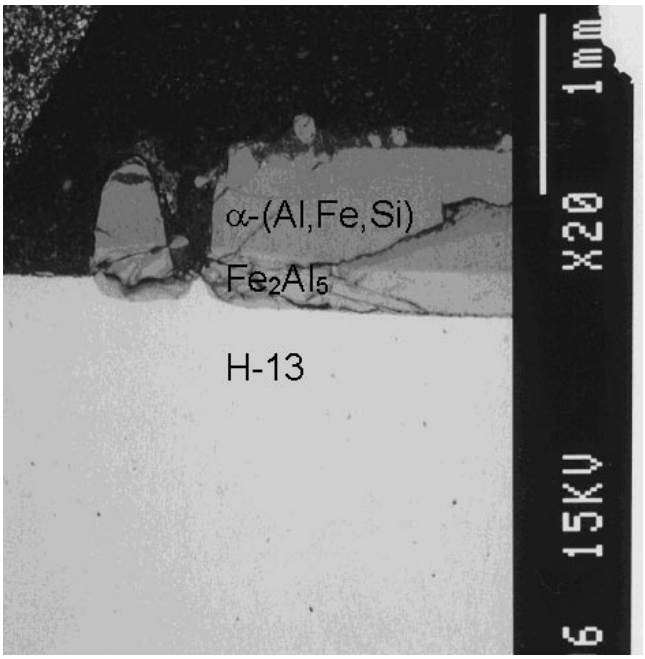

Fig. 8—Microstructure of the cross section of the diffusion couple (48 h) sample. The thickness of the intermetallic layer is smaller to that seen in the 1 week diffusion couple sample shown in Fig. 6. In addition, the thickness of the ternary phase is greater than the binary phase, contrary to that seen in the 1 week sample.

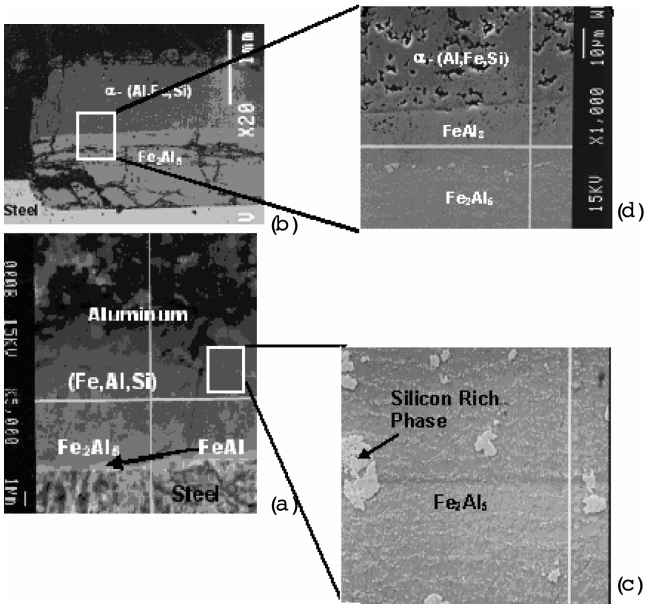

Fig. 9—Micrographs showing the comparison between the microstructure obtained from (*a*) and (*c*) soldered die insert from the die casting industry and (*b*) and (*d*) diffusion couple (1 week) performed in the laboratory. The die material in both cases was H-13 with similar heat treatment, and the cast alloy was aluminum 380.1.

is H-13, and the alloy is an industrial grade 380.1. Figure 6(a) shows the various layers that are formed between the steel surface and the aluminum alloy during diffusion. Figures 6(b), (c), and (d) show magnified microstructures of these intermediate phases. Figure 7 shows a low-magnification SEM image of the intermetallic layers. This sample was obtained by stripping the intermediate phase layers between the steel and the aluminum. Figure 6(a) is the cross-section SEM image showing the various layers of intermetallic phases between the steel and aluminum alloy. Figure 6(b) shows the ternary α-(Al,Fe,Si) phase. Energy peaks of manganese and zinc were also seen in the EDX spectrum of this layer. Manganese and zinc formed compounds on the phase boundaries of the ternary α-(Al,Fe,Si) phase. These compounds were mostly etched out during the extended diamond polishing and left behind pits on the phase boundaries, as seen in the image. Figure 6(c) shows the θ-Fe_4Al_{13} intermetallic-phase layer between the ternary and the binary Fe_2Al_5 phase. Figure 6(d) shows the binary iron-aluminum layer formed near the steel surface. Identity of the η-Fe_2Al_5 phase was confirmed through EDX analysis. Silicon was found as large precipitates in the binary phase region, at the grain boundaries, and at the interface. Energy peaks of chromium and sulphur were also picked up by the EDX of this layer. In Figure 7, the intermetallic layer was stripped off the steel (H-13) surface, and the pit formation is clearly evident. The intermetallic phases grow in a columnar pattern. The silicon precipitation can also be seen in the Fe_2Al_5 phase layer at the phase boundaries. The growth of the intermetallic layer continues until the cracks between adjacent pits in the intermetallic layer close, allowing no further aluminum melt access.

Figure 8 shows the microstructure of the diffusion zone cross section of a sample, which had undergone a 2-day (48 hours) diffusion reaction. This image also shows the presence of the intermediate layers but in various proportions of thickness as compared to the 1-week-long diffusion samples. Figure 9 shows a comparative analysis of the microstructures from a soldered sample obtained from the die casting industry along with the sample that underwent a 168-hours diffusion reaction.

Figure 9(a) is a sample from a die casting industry. It shows the intermetallic layers formed between steel and aluminum. Figure 9(b) is a sample from the diffusion couple between H-13 and aluminum alloy (168 hours). Figure 9(c) is an enlarged image of the binary η-Fe_2Al_5 phase in the microstructure shown in Figure 9(a). Notice the precipitation of the silicon-rich phase in this phase layer. Figure 9(d) is an enhanced image of the portion marked in Figure 9(b). This image shows the presence of a layer between η-Fe_2Al_5 and α-(Fe,Al,Si) phase layers, which is the θ-Fe_4Al_{13} phase. Also, notice the silicon-rich phase precipitating in the η-Fe_2Al_5 region. Figures 9(a) and (b) are digitally enhanced to clearly show the boundaries between the various phases.

Figure 10 shows the results of EDX spot-pattern analysis from the various spots across the diffusion-couple interface. The sample is from a 168-hours diffusion couple. The white line running across the micrographs represents the line on which each of the spots was present. The profile was obtained by spot EDX in a JEOL* 840 SEM using KEVEX**-Sigma software. The iron concentration was complimentary to the aluminum concentration, and it steadily decreased from the steel interface to the soldered aluminum. Figure 10(a) is the secondary electron imaging (SEI) image, showing the various layers of intermetallic compounds between the steel and the aluminum. Figure 10(b) is an enlarged portion (near

*JOEL is a trademark of Japan Electron Optics, Ltd., Tokyo, Japan.
**KEVEX is a trademark of Kevex Corporation, Foster City, CA.

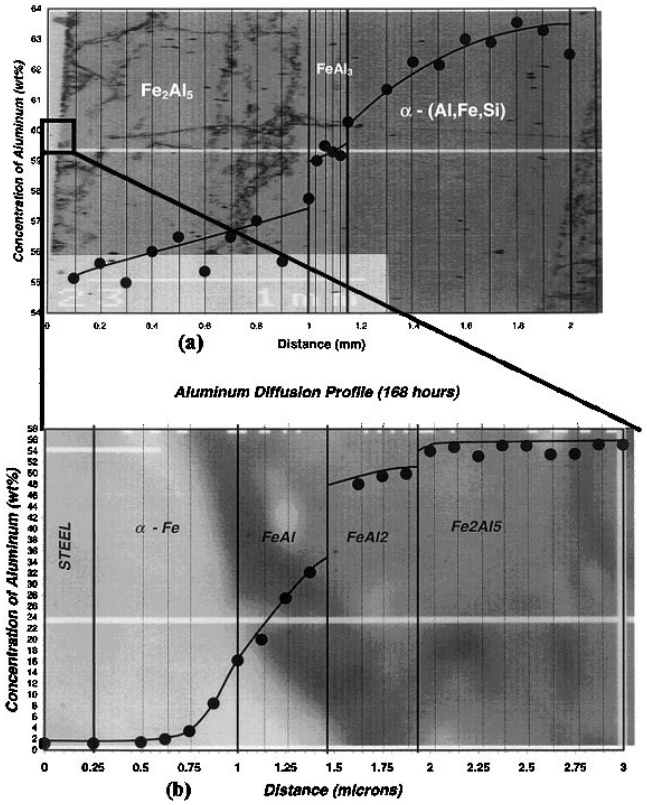

Fig. 10—Diffusion profiles from the diffusion couple held at 625 °C for 1 week (168 h). (*a*) Die soldered interface, showing the H-13 steel (left), intermediate phase layers, and the soldered aluminum alloy (right). (*b*) Enlarged region close to the steel surface (in (a)), showing the binary iron-aluminum compounds.

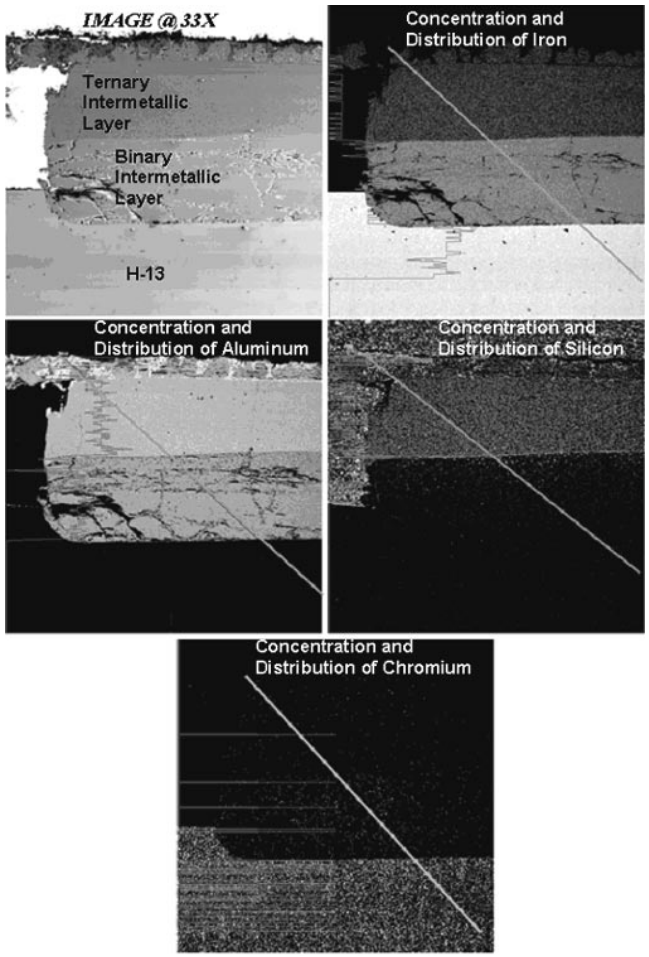

Fig. 11—Line-scan profiles on the microstructure from the diffusion couple (time = 1 week) of H-13 die material and molten aluminum A-380.1 alloy.

the steel interface) of the section shown in Figure 10(a). The various layers of iron-aluminum binary alloys formed close to the steel interface are evident.

Figure 11 shows the results of the X-ray mapping of the cross section of the sample that underwent 168-hours diffusion reaction. The distribution of iron, aluminum, silicon, and chromium are given. The profile was taken on the JEOL 840 SEM using the KEVEX-Sigma software. The image is of 1024 × 1024-pixel resolution, and the scanning was done on the straight line running across the microstructure. Data was analyzed on 1024 spots on the line running from the die material to the soldered aluminum. The residence time of the electron beam on each data point was 8 μs. The profile shows the active part of iron and aluminum in the first few layers from the steel surface. Binary compounds of iron and aluminum form first with chromium as the major impurity element. Chromium forms compounds and precipitates on the grain boundaries of the binary iron-aluminum compounds. Silicon exits as precipitates in the binary phases and at the interface between the binary and the ternary phases. Subsequently, a ternary α-(Al,Fe,Si) compound form with manganese as the major impurity element. Manganese forms compounds and precipitates on the grain boundaries of the ternary iron-aluminum-silicon phase.

Figure 12 shows the X-ray map of the microstructure of the sample that underwent a 48-hour diffusion reaction. The image was taken with a JEOL JSM-840 SEM. The distribution and concentration are shown in gradations of gray scales. The brighter the zone, the greater the concentration of the element in that region. The concentration profile was scanned across the thick line shown in each of the images. The image was acquired at the interface between the binary and the ternary phases in the intermetallic region. It can be observed that silicon is present at this interface as precipitates. Analyzing unpolished and polished regions of the layer explains the distribution of the minor elements, *i.e.*, zinc, manganese, chromium, *etc.*, and the cause of the porosity in the ternary phase. These elements exist primarily as precipitates in the ternary phase and the interface between the binary and the ternary phase, as can be seen from the two profiles given in the bottom of the image. These precipitates are eroded out of the phase layer due to corrosive action of aqueous medium during extensive polishing.

Figure 13 shows line scan profiles across a soldered interface of a sample acquired from a die casting company. These profiles were taken to confirm the results shown in Figure 10(b). The profile was taken with a JEOL JSM-840 SEM using the KEVEX-Sigma software. The image is of 1024 × 1024-pixel resolution, and the scanning was done on the straight line running across the microstructure. Data were analyzed on 1024 spots on the line running from the die material to the soldered aluminum. The residence time of the electron beam on each data point was 8 μs. The profile shows the active part of iron and aluminum in the

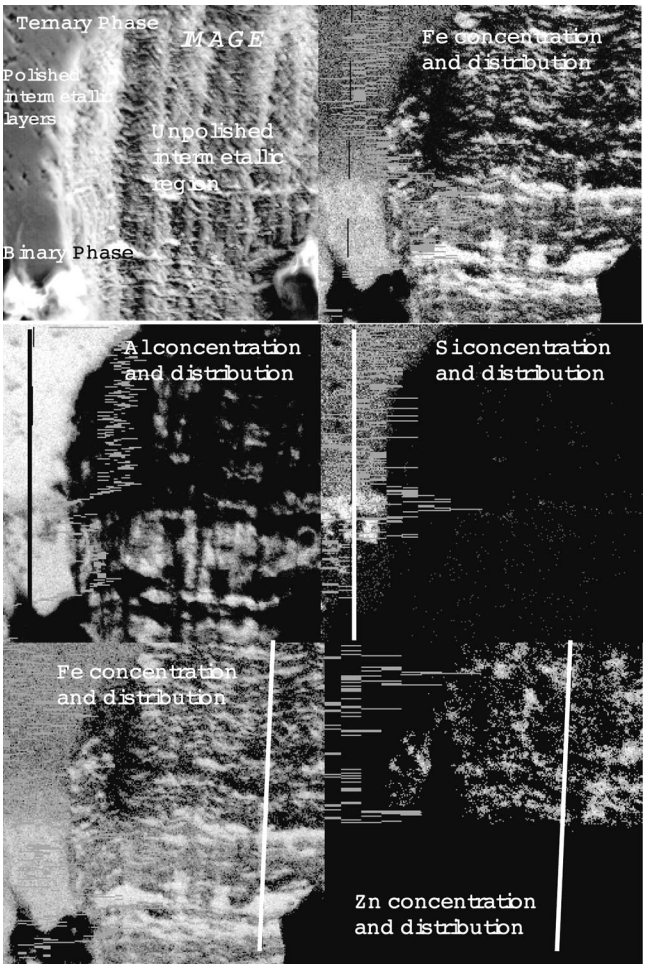

Fig. 12—The images show the distribution and the concentration line scan profiles of the respective elements in the intermediate layer. The image was taken at a region in the intermediate layer where a polished and an unpolished area coexisted. This map shows the distribution of the trace elements present in the multicomponent diffusion couple experiment

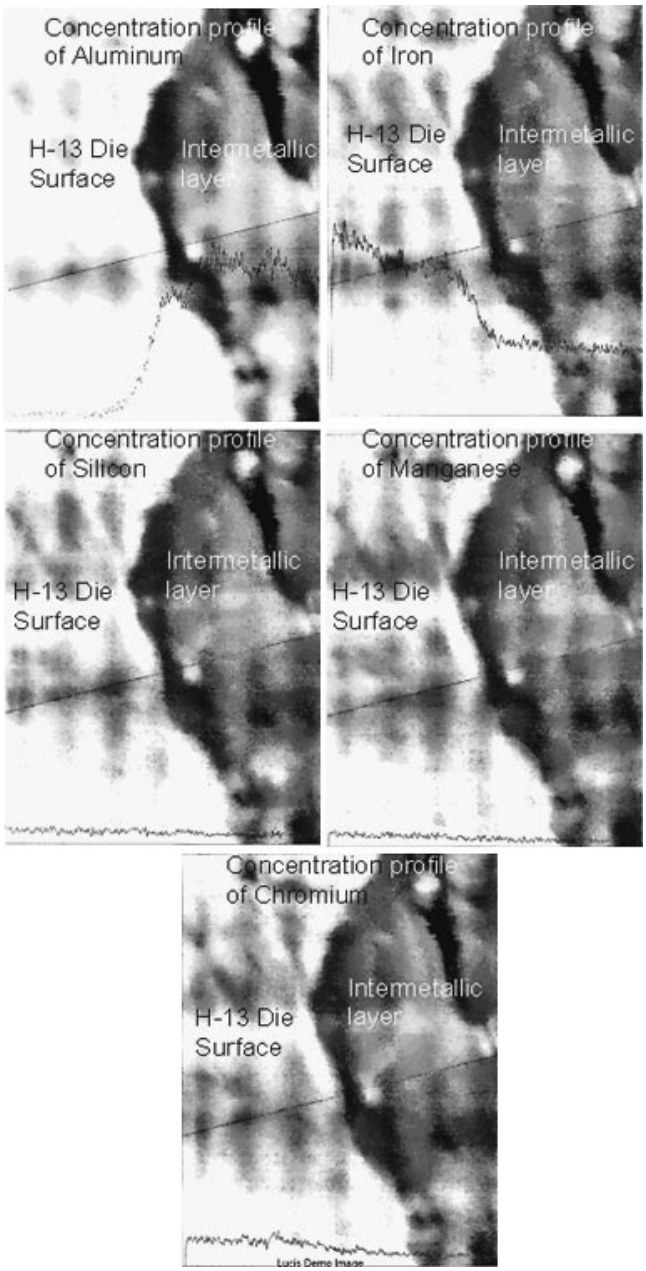

Fig. 13—Line-scan profiles on the microstructure of a soldered sample from an industrial die-casting operation. The die material here is H-13 and the molten metal is aluminum 380 alloy.

first few layers from the steel surface. Binary compounds of iron and aluminum form first with chromium as the major impurity element. Notice the presence of various binary Fe-Al compounds shown by the miscibility gaps.

Table II shows the result of the diffraction pattern obtained for the powder samples. The obtained "d-spacing" and the relative intensities of the pattern obtained are shown in the first two columns. The possible phases present and the lines for each of the observed d-spacing values are given. The d-spacing values for the phases were compared with the JCPDS card files: Fe_2Al_5-#47-1435; (Al,Fe,Si)-#20-0030; $Al_{13}Fe_4$-#47-1420; Al-#4-787; and Fe-#85-1410. Three compound structures matched most of the lines in the patterns obtained from all evaluated samples. These were Fe_2Al_5, Fe_4Al_{13}, and α-(Al,Fe,Si) phases. The respective lines of each phase are given against their respective d-spacing values. Only the very strong and strong peaks were considered from the pattern. Weak and very weak peaks were omitted because the strong peaks themselves were sufficient to confirm the phases present in the intermediate layers. The obtained d spacing for various compounds were within a 1 pct error margin to those obtained in the JCPDS files. The peaks from the X-ray pattern of the slant-polished samples matched well with that of the powder pattern. The sequence of the phases between the tool steel surface and the soldered aluminum follows the sequence observed in the metallographic analysis presented earlier. Table III shows the comparison of the lattice parameters calculated from the d spacing obtained from these experiments for each of the assumed phases, and the ones obtained for the phases from the JCPDS card files. The lattice parameters were calculated using the Cohen's method.[27] The structures of each phase were assumed to be that given in the respective card files.

Figure 14 shows the relation between the overall intermetallic-layer thickness and the square root of time of diffusion for the diffusion-couple experiments. The origin is taken as a valid data point in the curve because it is the initial condition for the diffusion process. The curve obtained is

Table II. X-Ray Diffraction Pattern of the Powder Sample of Intermertallic Layer Formed in the Diffusion Couple (Held for 168 Hours)

Powder Pattern of the Intermetallic Layers									
d-Spacing	Intensities	Phase	{*hkl*}	Phase	{*hkl*}	Phase	{*hkl*}	Phase	{*hkl*}
5.2767	13	—	—	—	—	α-(Fe,Al,Si)	{201}	—	—
4.9069	20	Fe2Al5	{110}	—	—	—	—	—	—
3.9722	26	—	—	—	—	α-(Fe,Al,Si)	{211}	—	—
3.9554	25	—	—	Fe4Al13	{211}	—	—	—	—
3.8413	16	—	—	—	—	—	—	—	—
3.8137	22	—	—	—	—	—	—	—	—
3.8041	17	Fe2Al5	{200}	—	—	—	—	—	—
3.2078	29	—	—	—	—	—	—	—	—
3.1978	34	Fe2Al5	{020}	—	—	—	—	—	—
3.1394	20	Fe2Al5	{111}	—	—	—	—	—	—
3.113	21	—	—	Fe4Al13	{131}	—	—	—	—
2.251	23	—	—	—	—	—	—	—	—
2.463	16	—	—	—	—	α-(Fe,Al,Si)	{316}	—	—
2.3628	18	—	—	—	—	—	—	—	—
2.3344	47	Fe2Al5	{310}	Fe4Al13	{051}	—	—	Al	{111}
2.3289	49	—	—	—	—	α-(Fe,Al,Si)	{317}	—	—
2.2912	23	—	—	Fe4Al13	—	α-(Fe,Al,Si)	{406}	—	—
2.2146	17	—	—	—	—	α-(Fe,Al,Si)	{325}	—	—
2.1512	55	—	—	—	—	α-(Fe,Al,Si)	{501}	—	—
2.1196	100	—	—	Fe4Al13	{511}	α-(Fe,Al,Si)	{30(10)}	—	—
2.0906	20	Fe2Al5	{221}	—	—	—	—	—	—
2.0857	0	Fe2Al5	{002}	—	—	—	—	—	—
2.0633	79	Fe2Al5	{311}	—	—	—	—	—	—
2.0499	48	Fe2Al5	{130}	Fe4Al13	{600}	α-(Fe,Al,Si)	{327}	—	—
2.0435	39	—	—	—	—	—	—	—	—
2.0354	87	—	—	—	—	α-(Fe,Al,Si)	{420}	Fe	{110}
2.0224	21	—	—	—	—	—	Al	{200}	
2.0176	21	—	—	—	—	—	—	—	—
1.9848	15	—	—	—	—	α-(Fe,Al,Si)	{417}	—	—
1.943	17	—	—	Fe4Al13	{431}	—	—	—	—
1.9062	10	Fe2Al5	{112}	Fe4Al13	{152}	α-(Fe,Al,Si)	{512}	—	—
1.8479	14	Fe2Al5	{400}	Fe4Al13	{413}	—	—	—	—
1.7646	14	Fe2Al5	{31}&{202}	—	—	—	—	—	—
1.7203	16	Fe2Al5	{022}	Fe4Al13	{701}	—	—	—	—
1.6138	13	—	—	—	—	—	—	—	—
1.5976	14	Fe2Al5	{040}	Fe4Al13	{603}	α-(Fe,Al,Si)	{42(10)}	—	—
1.5289	10	Fe2Al5	{222}	—	—	—	—	—	—
1.501	14	Fe2Al5	{21}&{331}	—	—	—	—	—	—
1.4763	10	—	—	Fe4Al13	{271}	—	—	—	—
1.475	18	Fe2Al5	{510}	Fe4Al13	{205}	—	—	—	—
1.4737	17	Fe2Al5	{240}	Fe4Al13	—	—	—	—	—
1.4721	14	Fe2Al5	{132}	—	—	—	—	—	—
1.4586	16	—	—	Fe4Al13	{244}	α-(Fe,Al,Si)	{00(18)}	—	—
1.4314	18	—	—	—	—	—	Fe	{200}	
1.4286	23	—	—	—	—	—	Al	{220}	
1.4038	16	—	—	Fe4Al13	{811}	—	—	—	—
1.3913	12	Fe2Al5	{402}	Fe4Al13	{461}	—	—	—	—
1.338	9	Fe2Al5	{241}	—	—	—	—	—	—
1.2686	33	—	—	—	—	α-(Fe,Al,Si)	{44(12)}	—	—

a straight line showing that the process is totally diffusion controlled. Although, the growth of the overall intermetallic layer follows the standard parabolic-rate law, the growth of the individual binary and ternary phases do not follow the parabolic-rate law. The rate constant for the growth of the intermetallic layer was calculated to be 0.1483 mm/hr$^{1/2}$. Hence, the rate equation was found to be $X = 0.15 \cdot t^{1/2}$, where X is the overall intermetallic-layer thickness, and t is the time in hours.

V. DISCUSSION

When the molten metal encounters the steel surface, the weak intergranular regions, which are devoid of the hard carbide phases, are attacked by the melt. This results in the formation of the primary solid solution of iron with aluminum, as per the phase diagram shown in Figure 15. The phase boundary attack, which is seen in Figure 5(a), results in the loosening of the steel grains, which eventually

Table III. Calculated and Theoretical Values of the Lattice Parameters of the Phases Given in Table II

		Calculated Lattice Parameters			Lattice Parameters in JCPDS		
Observed Phases	Unit Cell	*a*	*b*	*c*	*a*	*b*	*c*
Fe2Al5	orthorhombic	7.6148	6.3633	4.1959	7.6486	6.4131	4.2165
α-(Al,Fe,Si)	hexagonal	12.2368	—	28.2470	12.4000	—	26.1000
Fe4Al13	rhombohedral	—	—	—	14.2078	—	7.5472
		Percentage Change in Calculated Values from Observed Values					
Observed Phases	Unit Cell	*a*	*b*	*c*			
Fe2Al5	orthorhombic	−0.4419	−0.7765	−0.4886			
α-(Al,Fe,Si)	hexagonal	−1.3161	—	8.2261			
Fe4Al13	rhombohedral	—	—	—			

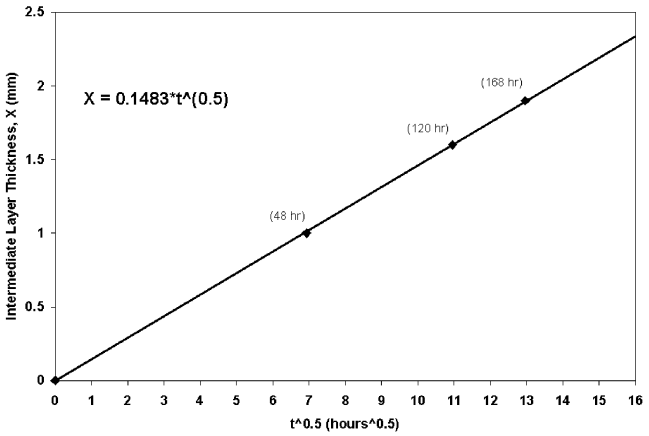

Fig. 14—Rate curve of the diffusion couple experiment. The rate of growth of the intermetallic layer obeys the parabolic rate law with the rate constant being 0.1483 mm/h$^{1/2}$.

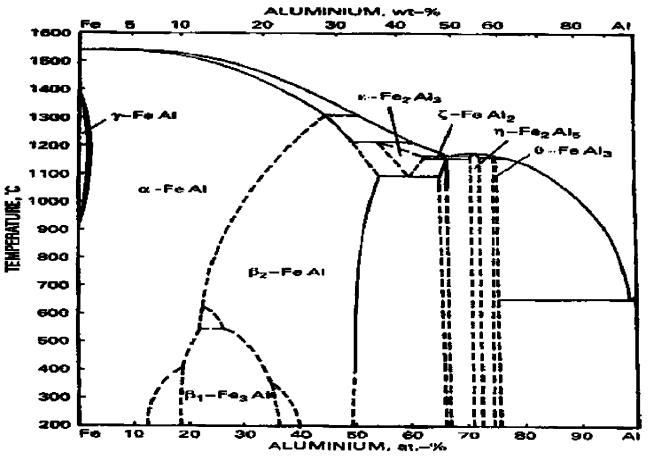

Fig. 15—Iron-aluminum binary phase diagram.[14]

separate from the surface due to the high drag forces of the incoming metal during casting. This gives rise to pits on the die surface. The iron from these pits and the loosened grains start to diffuse out resulting in the formation of a series of intermetallic compounds between aluminum and iron. Silicon and other impurity elements in the steel and the melt do not take part in the initial reactions because they are heavy elements and are not in sufficient concentrations to effectuate reaction phases. These minor elements precipitate as phases in the pits and in the adjoining binary phases of iron and aluminum. Figures 5(b) and 4(b) show the formation of the initial intermetallic phases in the erosion pits. Figures 5(c) and (d) are photographs of surfaces at the interface between the aluminum and steel. Soldered aluminum was mechanically stripped off the steel surface in one of the soldered samples from a commercial die-casting shop. Figure 5(c) shows the steel surface at the die/molten metal interface; the presence of erosion pits is quite evident. Figure 5(d) is the counterpart aluminum surface that was in contact with the steel surface. This image shows the intermetallic mounds on the aluminum. These intermetallic compound mounds were attached to the pits shown in Figure 5(c). These observations establish that a pit erosion process initiates soldering. This hypothesis has been reaffirmed by the results obtained in the diffusion-couple experiments.

Figures 4(d) and (f) show another critical feature in the steel/aluminum interface reaction. In these SEM images, the different stages of intermetallic layers growing, following the pitting process, can be observed. The intermetallic phases grow radially out of the erosion pits, forming pyramid-shaped intermetallic layers. Apart from the small portion of the initial, binary iron-aluminum phases, these intermetallic pyramids primarily consist of η-Fe_2Al_5 (close to the steel surface) and α-(Al,Fe,Si) phases (close to the soldered aluminum).

Two processes primarily govern the formation of the intermetallic layer in this stage. One is the diffusion of the iron atoms out of the steel surface through the intermetallic layers, causing the formation of the binary iron-aluminum intermetallic phases. The other process is the continuous reaction of the top layer of the binary phase with aluminum to form more binary and, finally, ternary intermetallic phases, as governed by the phase diagrams shown in Figures 15 and 16.

Initially, the growth of the ternary phase is more pronounced due to the rapid diffusion of the iron atoms and the rapid reaction with the available molten metal. The presence of fresh molten aluminum at every shot enhances the kinetics of formation of the ternary phase. Once these pits start to widen and merge with each other, as shown in Figures 4(c) and (e), the aluminum melt comes in contact with the steel surface only through the cracks and passages between two adjacent pits; hence, the growth of the binary η-Fe_2Al_5 compound is more pronounced. The reaction is driven by the diffusion of the iron atoms forming the binary η-Fe_2Al_5 rather than the chemical reaction with the aluminum melt. Thus, once the pits start to merge with each other and cut

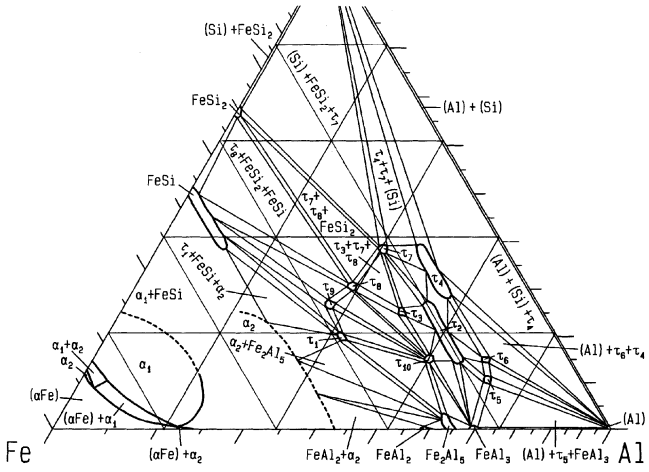

Fig. 16—Al-Fe-Si ternary system between 570 °C and 600 °C. Phase marked τ_5 is also known as α.[8]

off the supply of aluminum melt to the steel, the η-Fe_2Al_5 layer grows faster than the α-(Al,Fe,Si) layer. The growth of the intermetallic layer continues until all cracks close up, and this occurs roughly when the ratio of the thickness of the intermetallic layer and the soldered aluminum layer is 1:5. This explains the observation that most of the cross sections of pronounced soldering exhibit a ratio of 1:5.

Microstructural observations of the soldered samples from commercial die-casting shops and those from the controlled experimental work led to the hypothesis that soldering is a diffusion-driven process. This hypothesis is supported by the diffusion-couple experimental results.

The microstructures shown in Figures 6 and 8 reveal that iron is the primary diffusing species in the system. This is shown by the growth of the diffusion products out of the steel surface rather than into the steel. Also, EDX analysis and X-ray diffraction patterns of the phases in the intermediate layers reveal that the layer closest to the steel surface is most likely a series of binary iron-aluminum phases dictated by the iron-aluminum phase diagram shown in Figure 15, and the layer closest to the aluminum side is most likely a ternary α-(Al,Fe,Si) phase dictated by the ternary Al, Fe, and Si system shown in Figure 15. Figures 6(b), (c), and (d) show magnified SEM images of the portions shown in Figure 6(a). There was a relatively thin layer of intermetallic phase found between the binary and the ternary phases. This is the binary θ-$FeAl_3$ (existing as Fe_4Al_{13}) phase with the presence of various impurity elements from the steel and aluminum alloy. The composition of iron and aluminum was similar to the θ-Fe_4Al_{13} phase as found by the X-ray diffraction techniques shown in Table II. The large binary phase near the steel interface is the η-Fe_2Al_5 phase. This was affirmed by X-ray diffraction on the powder sample obtained from the intermetallic layers in addition to the EDX analysis of the region in the soldered and diffusion microstructures. The ternary phase closest to the aluminum side of the microstructure is the α-(Al,Fe,Si) phase. This was indicated by the EDX analysis of various microstructures and the X-ray pattern. In Figure 6(a), the ternary phase is rather porous as compared to the other phases. This porosity would have occurred due to the corrosion of the phases present in those areas.

Figure 12 shows an X-ray mapping image of the polished surface and unpolished region of the intermetallic layers. The unpolished layer does not show any porosity. Instead, the maps show that these areas were occupied by a zinc and iron-rich intermetallic phase. Polishing in an aqueous medium for three to four weeks resulted in the corrosion of this phase and resulted in porosity. Figure 7 shows the cross section of an intermetallic layer between steel and aluminum that was separated mechanically. The growth pattern of the intermetallic layers can be deciphered from this micrograph. It can be seen that the intermetallic layers grew in a columnar fashion, away from the steel surface. Silicon was present as precipitates in the binary iron-aluminum phase, as shown in Figures 6(c), 7, and 9(c). Silicon-rich phases precipitated at the grain boundaries of the binary Fe_2Al_5 phase layer, and the large star-shaped silicon precipitates were pushed to the boundary between the binary and the ternary phase layers in the microstructure (Figures 6(b), (c), and 9(c)). Figure 9 shows a comparison of the microstructural features of the diffusion sample and a soldered sample from industry. The growth patterns and the compositions of the intermetallic phases are similar. The data confirm that the mechanism of soldering is a diffusion-driven process.

The hypothesis that binary iron-aluminum intermetallic phases grow near the steel interface followed by a ternary α-(Al,Fe,Si) compound is confirmed by the concentration profiles shown in the Figure 10. Despite a 5 pct variation due to inaccuracies in the background subtraction of the peaks generated by the EDX analysis software, one can safely state that all the phases present in the binary iron-aluminum phase diagram (Figure 15) are present in the soldered intermediate layers. The presence of these phases is clearly demarcated by the miscibility gaps corresponding to the intermediate, immiscible two-phase regions of the binary phase diagram. The variation in the values obtained by the EDX spot analysis is no less than 10 pct of those found in the phase diagram. This can be attributed to the fact that a perfect background subtraction of the X-ray peaks is not available and that the lattice of the binary compounds contain impurity elements, such as chromium and manganese, which tend to decrease the effective percentages of iron and aluminum during the quantitative analysis of the EDX spectrums. Line-scan concentration profiles, shown in Figures 11 and 13, reveal that chromium is a major impurity in the η-Fe_2Al_5 phase and that manganese is a major impurity in the α-(Al,Fe,Si) phase. The calculated lattice parameters of these two phases revealed that the unit cell of the orthorhombic η-Fe_2Al_5 phase is extended along the c axis, as expected, due to the presence of impurity elements, such as chromium atoms.

From the analysis of the results of the diffusion-couple experiments, the microstructural analysis of soldered samples from industrial sites, and our experimental matrix, it can be concluded that the mechanism of die soldering is primarily diffusion-driven. The phases in the intermediate intermetallic layer between steel and aluminum have been positively identified based on this analysis.

VI. CONCLUSIONS

The analysis of the metallurgy and kinetics of the soldering phenomenon lead to the following conclusions.

1. Soldering is primarily a diffusion-driven phenomenon.

Diffusion of iron atoms from the ferrous die into the aluminum melt causes the formation of a series of binary and ternary intermetallic phases onto which the aluminum alloy solders.

2. Laboratory die-soldering experiments, as well as diffusion-couple experiments between the ferrous die material and aluminum melt, established the metallurgy of the aluminum/steel die interface reactions.
   a. Initially, a series of iron-aluminum binary phases form. The largest volume fraction of binary phase formed is η-Fe_2Al_5. Above the binary phases, the ternary α-(Fe,Al,Si) phase forms. A layer of θ-Fe_4Al_{13} forms between the η-Fe_2Al_5 and α-(Fe,Al,Si) phase layers.
   b. Silicon precipitates on the grain boundaries of the η-Fe_2Al_5 phase layer and at the interface boundary between the binary η-Fe_2Al_5 and the ternary α-(Fe,Al,Si) phase layers.
   c. Zinc, manganese, and other minor elements added to the aluminum melt precipitate on the grain boundaries of the ternary α-(Fe,Al,Si) phase layer.
   d. Chromium, vanadium, and other minor elements present in H-13 tool steel precipitate as phases in the binary η-Fe_2Al_5 phase layers.
   e. Soldering is a diffusion-driven process and the growth kinetics adhere to the parabolic law. The rate equation is $X = 0.15 \cdot t^{1/2}$, where X is the overall intermetallic layer thickness in mm, and t is the time in hours.
3. A mechanism has been established for the reaction between molten aluminum and the ferrous die; the mechanism consists of five stages:
   a. erosion of phase boundaries on the die surface;
   b. pitting of the die surface;
   c. formation of iron-aluminum compounds and formation of pyramid-shaped structures of intermetallic phases;
   d. adherence of aluminum on the pyramids of intermetallic phases; and
   e. straightening of erosion pits and intermetallic phases.

This knowledge base establishes the physical metallurgy of the interfacial reactions between molten aluminum and H-13 die steel. These results explain the transport phenomena controlling the 1:5 ratio observed between the intermediate phase layer and the total soldered layer coexisting on top of the die surface irrespective of the number of shots during die casting.

REFERENCES

1. M. Yu, Yeou-Li Chu, and R. Shivpuri: Ohio State University, Columbus, OH, unpublished research, 1997.
2. R. Shivpuri, S.J. Chang, Y.I. Chu, and M. Kuthirakulathu: *Transactions of the North American Die Casting Association (NADCA) Congr. and Exp.*, Sept. 30–Oct. 3, 1991, NADCA, Rosemont, IL, p. 391.
3. M. Yu, R. Shivpuri, and R.A. Rapp: *J. Mater. Eng. Performance*, 1995, vol. 4 (2), p. 175.
4. M. Yu, R. Shivpuri, R.A. Rapp, and Murali Ranganathan: Madison-Kipp, Madison, WI, private communication, 1997.
5. Y.L. Chu, K. Venkatesan, J.R. Conrod, K. Sridharan, M. Shamim, R.P. Fetherston, R. Shivpuri, and Murali Ranganathan: Madison-Kipp, Madison, WI, private communication, 1997.
6. H.G. Munson and T.H. Camel: *Transactions of the North American Die Casting Association (NADCA) Congr. and Exp.*, Sept. 30–Oct. 3, NADCA, Rosemont, IL, 1991.
7. Y. Naerheim and E.R. Hennie: *Foundry Trade J.*, 1980, Jan., pp. 11-15, and 30.
8. L.A. Norström and B. Klarenfiord: *Transactions of the North American Die Casting Association (NADCA) Congr. and Exp.*, NADCA, Rosemont, IL, 1993, p. 75.
9. Y.L. Chu, P.S. Cheng, and R. Shivpuri: *Transactions of the North American Die Casting Association (NADCA) Congr. and Exp.*, NADCA, Rosemont, IL, 1993, p. 124.
10. K. Wladyslaw and F. Alexander: *Transactions of the North American Die Casting Association (NADCA) Congr. and Exp.*, NADCA, Rosemont, IL, 1993, p. 34.
11. S. Shankar and D. Apelian: *Transactions of the North American Die Casting Association (NADCA) Congr. and Exp.*, NADCA, Rosemont, IL, 1997, Nov., p. 245.
12. S. Shankar and D. Apelian: *Proc. AFS 5th Int. Molten Metal Conf.*, NADCA, Rosemont, IL, 1998, Nov., p. 281.
13. S. Shankar and D. Apelian: *Transactions of the North American Die Casting Association (NADCA) Congr. and Exp.*, NADCA, Rosemont, IL, Nov. 1999.
14. R.W. Richards: *Int. Met. Rev.*, 1994, vol. 39(5), p. 191.
15. S. Denner and Y.W. Kim: *High Temperature Protective Coatings*, S.C. Singhal, ed., p. 233.
16. G. Eggler, W. Auer, and H. Kaesche: *J. Mater. Sci.*, 1986, vol. 21, pp. 3348-50.
17. J.H. Nicholls: *Corr. Technol.*, 1964, Oct., p. 16.
18. T. Heumann and S. Dittrich: *Z. Metallkd.*, 1959, vol. 50, p. 167.
19. A.K. Kurakin: *Fiz. Met. Metalov.*, 1970, vol. 30, p. 430.
20. N. Komatsu, M. Nakamura, and H. Fujita: *J. Jpn Inst. Met.*, 1981, vol. 45, p. 416.
21. G. Langenschied and G. Klein: *Prakt. Metallo.*, 1970, vol. 14, p. 251.
22. V.N. Yeremenko, Y.V. Natanzon, and V.I. Bybkov: *J. Mater. Sci.*, 1982, vol. 16, p. 1748.
23. D.I. Lainer and A.K. Kurakin: *Fiz. Met. Metalov.*, 1964, vol. 18, p. 145.
24. M.V. Akdeniz, A.O. Mekhrabov, and T. Yilmaz: *Scripta Metall. Mater.*, 1994, vol. 31, p. 1723.
25. C. Wagner: *Thermodynamics of Alloys*, Addison-Wesley Publishing Company, Inc., Reading, MA.
26. K. Holz Earl: *Transactions of 7th SDCE Int. Die Casting Congr.*, Oct. 16–19, 1972.
27. B.D. Cullity: *Elements of X-ray Diffraction*, 2nd ed., Addison-Wesley Publishing Company, Inc., Reading, MA.